Electronic Journal of University of Aden for Basic and Applied Sciences
EJUA-BA Vol. 3 No. 3 (2022)
https://doi.org/10.47372/ejua-ba.2022.3.185
ISSN: 2708-0684

RESEARCH ARTICLE

IMPLICATIONS OF MANTLE XENOLITHS IN THE PLIOCENE-QUATERNARY BASALTS FROM THE SHAWRAN CRATER, BIR ALI AREA, YEMEN

Abdelmonem M. Habtoor[1,*], Ibrahim A. Al-Akhaly[2] and Ali S. Lashdaf[3]

[1] *Dept. of Engineering Geology, Faculty of Oil and Minerals, University of Shabwah, Shabwah, Yemen*
[2] *Dept. of Geology, Faculty of Petroleum and Natural Resources, University of Sana'a, Sana'a, Yemen*
[3] *Geological Survey & Minerals Resources Board, Shabwah Branch, Yemen*

***Corresponding author: Abdelmonem M. Habtoor; E-mail: abdelmonemhabtoor@gmail.com**

Received: 24 August 2022 / Accepted: 25 September 2022 / Published online: 30 September 2022

Abstract

Mantle xenoliths in basalt and tuffaceous volcanoes at the Shawran Crater, Bir Ali area, along the southeastern coast of Yemen are very useful to elucidate the nature of the lithospheric mantle beneath the area, which is characterised by rift tectonic activity and volcanism during the Pliocene–Quaternary period. The studied mantle xenoliths are mostly fresh showing igneous textures and composed mainly of spinel harzburgite and lherzolite, in addition to, less prominently, dunite. Spinel harzburgite and lherzolite are holocrystalline with abundant granular spinel that occurs interstitially to olivine, orthopyroxene, and clinopyroxene. The forsterite content of olivine is high ($Fo_{89–91}$) attesting its mantle residue origin. Orthopyroxene is mostly enstatite ($En_{89–92}$), and clinopyroxene is diopsidic in composition ($Wo_{24–47}En_{49–52}$ $Fs_{2–4}$). Spinel Cr# (Cr/(Cr + Al) is distinguishable between lherzolites (Cr# = 0.12–0.15) and harzburgites (Cr# = 0.20–0.31). The calculated oxygen fugacity ($\log fO_2$) of the studied lherzolites (−1.76 to −0.20) and harzburgite (−2.7 to −0.98) xenoliths, and their equilibration temperature (~ 820–1,145°C) at about 1.5 GPa pressure, along with their mineralogical and petrological characteristics, are all support their evolution by mixed enrichment from a fertile and depleted asthenospheric mantle beneath the Bir Ali area.

Keywords: Ultramafic xenoliths, Spinel harzburgite, Depleted asthenosphere, Bir Ali volcanics, Yemen.

Introduction

Mantle xenoliths entrained in alkali basalt and tuffaceous volcanoes are an important source of information about the composition and nature of the Earth's upper mantle [1, 2]. The xenolith types are interpreted to reflect a primarily fertile mantle or a depleted mantle that represents residues after modern to ancient melt extraction [1, 2, 3, 4, 5]. In general, alkali basalts are widespread in continental plate interiors and are usually associated with continental rifting [6]. They represent relatively small degrees of partial melting of deep mantle sources and are the main host of mantle xenoliths [7,8], while the presence of xenoliths suggests fast ascent from great depths [9,10]. reported that the recent basalts of the Ethiopian rift were produced as small degrees of partial melting predictive at 15–25 Kbar.

Al-Fugha and Al-Amaireh [11] studied basaltic rocks containing abundant upper mantle xenoliths (spinel lherzolite, harzburgite, and olivine websterite) from northeastern Jordan volcanoes. These xenoliths contain olivine, orthopyroxene, clinopyroxene, and trace amounts of spinel. Their mineral assemblages indicate that they were derived and equilibrated under upper mantle conditions within a temperature range of 970-1,090°C.

Ahmed et al. [2] studied fresh ultramafic xenoliths hosted by basanite lava in the Harrat Kishb area, which is a part of the Cenozoic volcanic fields in the western margin of the Arabian Shield, to evaluate the nature and petrogenetic processes involved in the evolution of the lithospheric mantle beneath the Arabian Shield. They found that the majority of the mantle xenoliths (~92%) are peridotites (lherzolites and pyroxene-bearing harzburgites) and display a magmatic proto-granular

texture. These peridotite xenoliths represent residues after variable degrees of melt extraction from a fertile mantle.

Al-Mishwat and Dawod [12] classified xenoliths from the Ghab Pliocene volcanic field in northwestern Syria into a spinel peridotite type, including lherzolite and harzburgite. These consist of forsterite, enstatite, and chromium diopside, and have a medium-grained equi-granular texture. They suggested that the petrological processes involve partial melting of the mantle source, crystallisation of basaltic liquids during their ascent to the surface, and crystallisation at shallow depths and on the surface.

The Quaternary volcanoes in Yemen were generated and developed through the post-rift stage (Miocene to Recent) [13]. Volcanic cones, domes, sheets, and lava flows are typical occurrences of these volcanoes. They are mainly composed of basaltic lavas, stratified basic tuffs and agglomeratic pyroclastics, and less common differentiated rock types, except the Al-Lisi volcano (5 km east of Dhamar City), which is entirely composed of rhyolitic lava flows [14]. There are eight well-known volcanic fields situated along the Gulf of Aden coast. They are mainly composed of individual volcanoes characterised by central vent eruptions. There are geological, chronological, and geochemical differences among those outcropping the west and east of Aden [15]. Those in the west of Aden are older (10–5 Ma) – including the Island of Perim, Jabal Kharaz, Jabal Al-Birkah, Ras Imran, Little Aden, and Aden – and are stratoid volcanoes characterised by transitional mildly alkaline basalt to peralkaline rhyolite. Those in the east of Aden are younger (5–0 Ma) and include Shuqrah (Al Urkoob-Ahwar), Bir Ali, and Ataq as well as smaller basaltic fields in Hadramawt and Al-Mahrah in the farther east (Qusaier, Er-Raidah, Musayna'h-Hadhathem, Hesay-Thamnoon, and the southern part of Wadi Al-Masilah) and the inland volcanic fields (Sana'a-Amran, Marib-Sirwah, and Dhamar-Rada'a) (Fig. 1). They are low cones (basalts and basic pyroclastics), mostly characterised by an alkaline affinity [14].

Peridotite xenoliths are found in the Balhaf–Bir Ali volcanic field in southern Yemen [16, 17, 18, 19, 20]. The Balhaf–Bir Ali volcanic field is located approximately between the co-ordinates 48°00′10″–48°00′30″E and 13°00′58″–14°00′10″N. It is about 130 km southwest of Al-Mukalla City and 450 km northeast of Aden City (Fig. 1). In this study, we describe the petrographic characteristics and mineral composition of peridotite xenoliths, along with thermometric and oxidation state data, from the Shawran Crater in the Bir Ali volcanic field on the southeastern coast of Yemen to try characterize the nature and thermal state of the mantle beneath this part of Yemen.

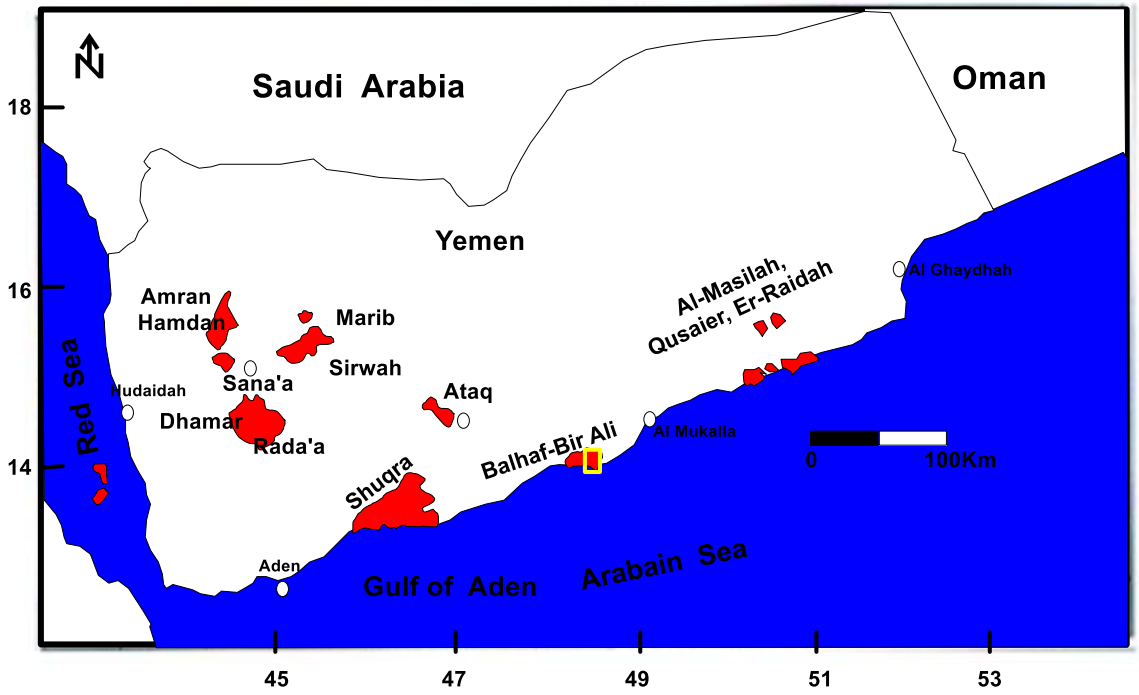

Fig. 1: Location map showing the distribution of Quaternary volcanic fields of Yemen (Modified after [14, 19, 21]. The study area is bounded by square.

Geological setting

The Balhaf–Bir Ali volcanic field (covering ~500 km^2) contains young basaltic lava that formed during 5–0 Ma [14]. It is represented by numerous cinder cones and lava flows. They are composed of basalts and basaltic scoria cones, tuffaceous materials in combination with pyroclastic rocks consisting of ashes and tuff rings. Columnar jointing and "aa" lava are clearly exposed within the volcanic lava. The Shawran Crater is located about 3 km east of Bir Ali and is considered as one of the youngest eruptions in the field (Fig. 2). The landward lip of this crater reaches an elevation of about 200 m above sea level. This crater covers ~ 800 m^2 and is probably similar to those found in Hawaiian Island volcanoes [19].

The crater walls are composed of basaltic scoria intercalated with tuffaceous trachytes that have been cemented by calcareous materials [19]. Ejected materials found on the foothills includes pebbles of peridotite xenoliths and olivine basalt. The largest peridotite xenoliths collected from the Shawran Crater that mainly consist of tuffaceous trachytes with intercalated basaltic scoria (Fig. 3a, b). Most of the peridotite xenoliths hosted within basaltic scoria and tuffaceous trachytes vary in diameter from 10 to 30 cm on the longest axis (Fig. 3a–d). The hand specimen colour of the fresh xenoliths is pale green with a proto-granular texture (Fig. 3b–f). The mantle xenoliths are spinel harzburgites [19] and lherzolites [17, 20, 21, 22].

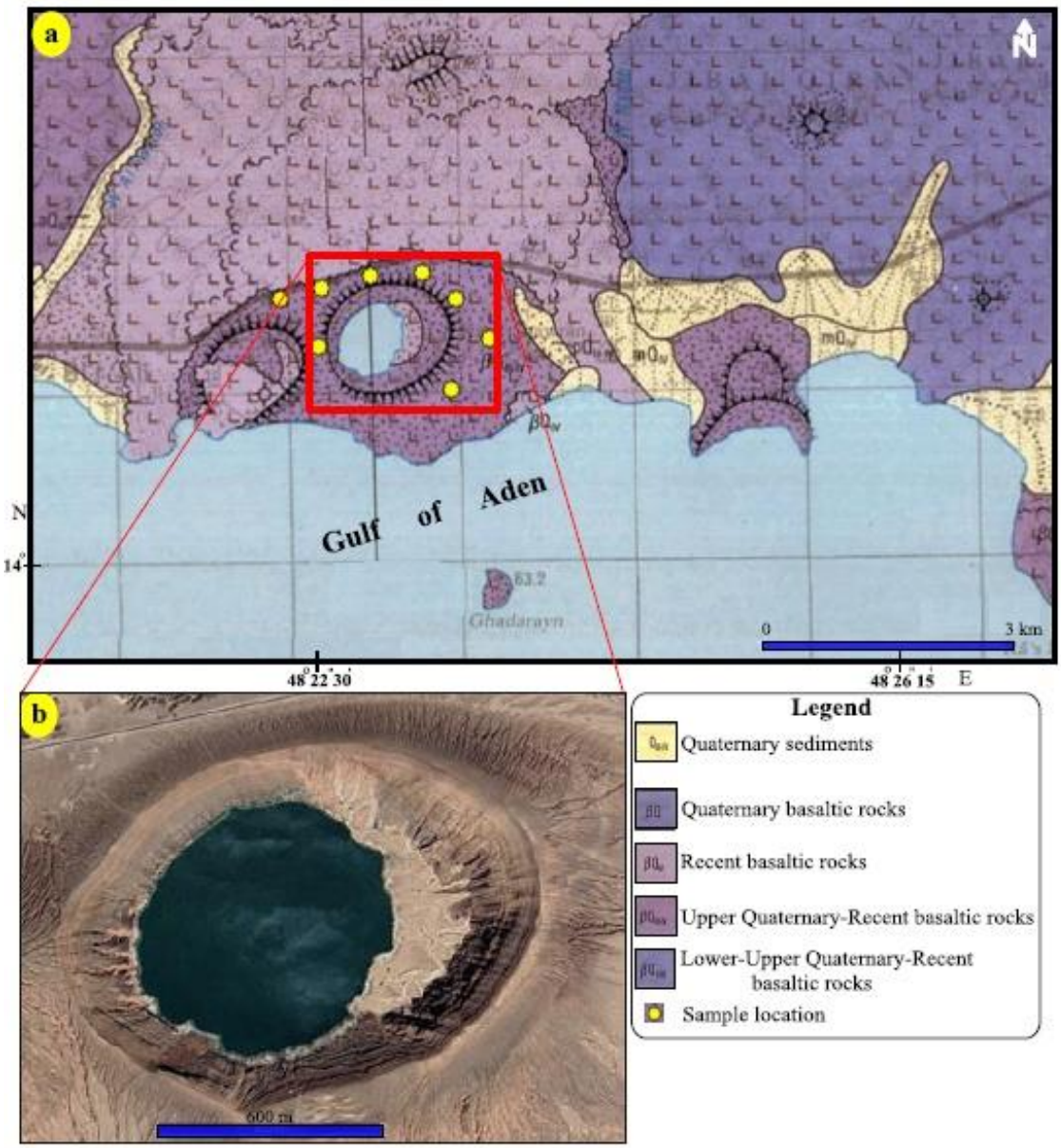

Fig. 2: a Geologic map showing the main volcanic units in Bir Ali volcanism (after [16].
b Close google earth view of the Shawran crater.

Sampling and analytical techniques

Ten fresh representative samples were collected from the Shawran Crater, Bir Ali area, for petro-graphical and mineralogical analyses, six of them were selected for mineral chemistry studies. Thin sections were prepared and subsequently investigated under transmitted and reflected optical microscopy. The selected samples were chosen for mineralogical analysis using a JEOL electron-probe micro analyser (EPMA) JXA-8200 at the Department of Mineral Resources and Rocks, Faculty of Earth Sciences, King Abdulaziz University, Jeddah, Saudi Arabia. The analytical conditions were 15 kV accelerating voltage, 20 nA probe current, and 3 µm beam diameter. The raw data were corrected with an online ZAF correction program. The amounts of Fe^{3+} and Fe^{2+} in spinel were calculated assuming spinel stoichiometry. The selected microprobe analyses of the minerals are presented in Tables 1–4.

Petrography

Microscopic studies of the peridotite xenoliths showed that they consist of olivine, orthopyroxene, clinopyroxene, and spinel (Fig. 4). All the constituent phases are homogeneous, without chemical zoning. Orthopyroxene is subhedral, varying in size from 0.2 to 0.4 mm (Figs 4a–f). Some orthopyroxene contains lamellae of clinopyroxene, whereas clinopyroxene is anhedral to subhedral and as interstitial phases between olivine and orthopyroxene (Fig. 4e, f). Olivine occurs as coarse-grained crystals (up to 0.2 mm in size) with Y-shaped cracks and undulose extinction (Fig. 4d). Spinel appears as reddish-brown, anhedral crystals and is found as interstitial phases among other minerals (Fig. 4e, f).

Mineral Chemistry

Electron microprobe analysis was carried out on four mineral phases – olivine, orthopyroxene, clinopyroxene, and spinel – as they represent the main constituents of the studied xenoliths (Tables 1–4).

Olivine

The olivine composition in spinel harzburgites is homogeneous with an average forsterite (Fo) content (Fo = 100 × Mg/(Mg + Fe^{2+}) atomic ratio) of Fo_{91} (ranges from 0.89 to 0.91). Its CaO content ranges from 0.05 to 0.08 wt.%, NiO content from 0.30 to 0.45 wt.%, FeO content from 8.74 to 9.03 wt.%, MnO content from 0.05 to 0.18 wt.%, and MgO content from 49.40 to 50.36 wt.% (Table 1). The olivine composition in lherzolite is also homogeneous with limited range of Fo content, ranging from Fo_{89} to Fo_{90}. The CaO content ranges from 0.01 to 0.13 wt.%, relatively high compared to spinel harzburgites. The NiO content varies from 0.30 to 0.41 wt.%, FeO content from 9.70 to 10.98 wt.%, MnO content from 0.11 to 0.20 wt.%, and MgO content from 48.05 to 49.41 wt.% (Table 1). According to their Fo and CaO contents, most of the olivine from spinel harzburgites is plotted within the depleted (refractory) mantle field, while all olivine from lherzolite is plotted in the fertile mantle field (Fig. 5a).

Orthopyroxene

Orthopyroxene is a major constituent of spinel harzburgites. It is mainly enstatite in composition (Wo_1 $En_{89–91}$ $Fs_{9–10}$) (Table 2). Orthopyroxene shows a restricted range of high Mg# (0.91–0.92), similar to those of the depleted mantle peridotite xenoliths (average Mg# = 0.92) (Table 2). The CaO content ranges from 0.68 to 0.77 wt.%, NiO content from 0.01 to 0.08 wt.%, FeO content from 5.21 to 5.61 wt.%, MnO content from 0.10 to 0.14 wt.%, and MgO content from 33.38 to 33.87 wt.% (Table 2). Orthopyroxene in lherzolite is also enstatite in composition ($Wo_{1–2}$ $En_{90–91}$ $Fs_{6–8}$). The Al_2O_3, Cr_2O_3, FeO_t, Na_2O, and CaO contents of orthopyroxene from lherzolite are similar to those of spinel harzburgites (Table 2).

Clinopyroxene

Clinopyroxene in spinel harzburgite is mainly diopside in composition (Wo_{47} $En_{49–50}$ $Fs_{3–4}$) with very restricted Mg# = 0.93–0.94 [Mg# = Mg/(Mg + Fe^{2+})] value. Cr_2O_3 varies from 0.92 to 2.04 wt.%, Al_2O_3 from 4.51 to 6.10 wt.%, and higher TiO_2 content that ranges from 0.19 to 0.96 wt.% (Table 3). The clinopyroxene from spinel harzburgite trends into the refractory field (Fig. 5b). Clinopyroxene in lherzolite is also diopsiditic in composition ($Wo_{46–48}$ $En_{50–52}$ $Fs_{2–3}$) with Mg# = 0.92, and Cr_2O_3 varies from 0.58 to 0.77 wt.%. The Al_2O_3 content of clinopyroxene ranges from 4.89 to 5.52 wt.%, and high TiO_2 content ranges from 0.32 to 0.77 wt.%. The clinopyroxene from lherzolite trends into and close to the fertile mantle field (Fig. 5b).

Spinel

Representative analyses of spinel from the investigated spinel harzburgite and lherzolite samples are given in Table 4 and are remarkably homogeneous for each sample. Spinel from spinel harzburgite has low Cr# (0.20–0.31), high Mg# (0.79–0.81), and low TiO_2 content (0.02–0.07 wt.%). It is mostly aluminous in composition; the Al_2O_3 content ranges from 42.10 to 49.22 wt.% (45.96 wt.% on average), and Cr_2O_3 ranges from 19.43 to 28.03 wt.% (24 wt.% on average). Meanwhile, spinel from lherzolite contains much lower Cr# (0.12–0.15) compared with spinel harzburgite, both of them have comparable Mg# (0.75–0.83) as well as TiO_2 (0.07–0.16 wt.%). Spinel in lherzolite is more Al_2O_3 rich than spinel harzburgite, it ranges from 53.10 to 56.98 wt.% (55.04 wt.% on average), and Cr_2O_3 ranges from 11.38 to 14.8 wt.% (13.09 wt.% on average).

The high Mg# and very low Cr# in lherzolite were plotted in the field of fertile peridotites, whereas the relatively higher Cr# and low Mg# harzburgite were plotted in close proximity to the refractory peridotite field (Fig. 5c). All spinel harzburgites and lherzolites in this study are plotted within the low Cr# field in the olivine-spinel mantle array (OSMA) [23] (Fig. 5d) and fall within the field defined for abyssal peridotites [24].

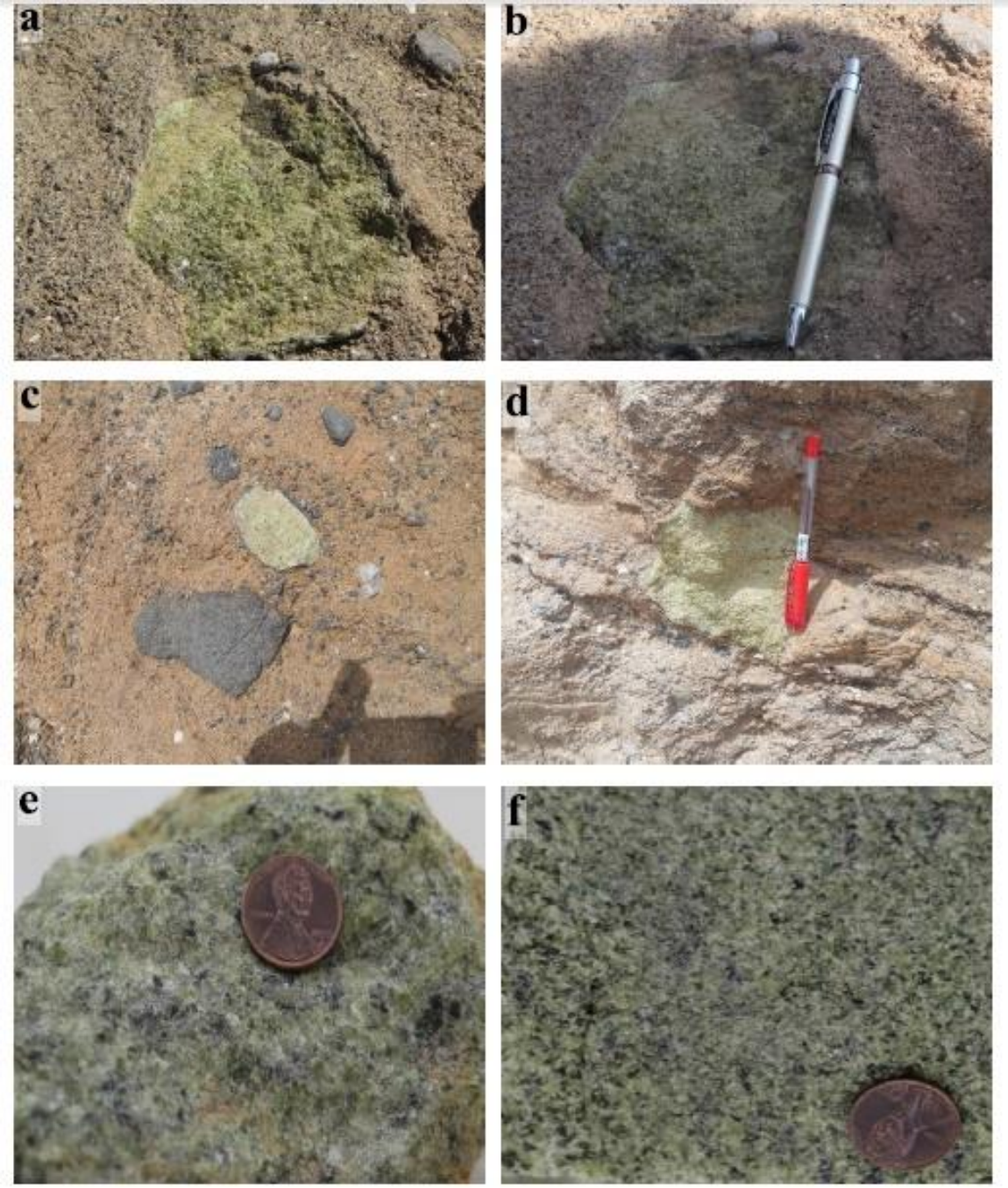

Fig. 3: a-d Hand specimens of mantle xenoliths showing greenish fresh color of peridotite xenoliths. **e** Spinel harzburgites. **f** Lherzolite.

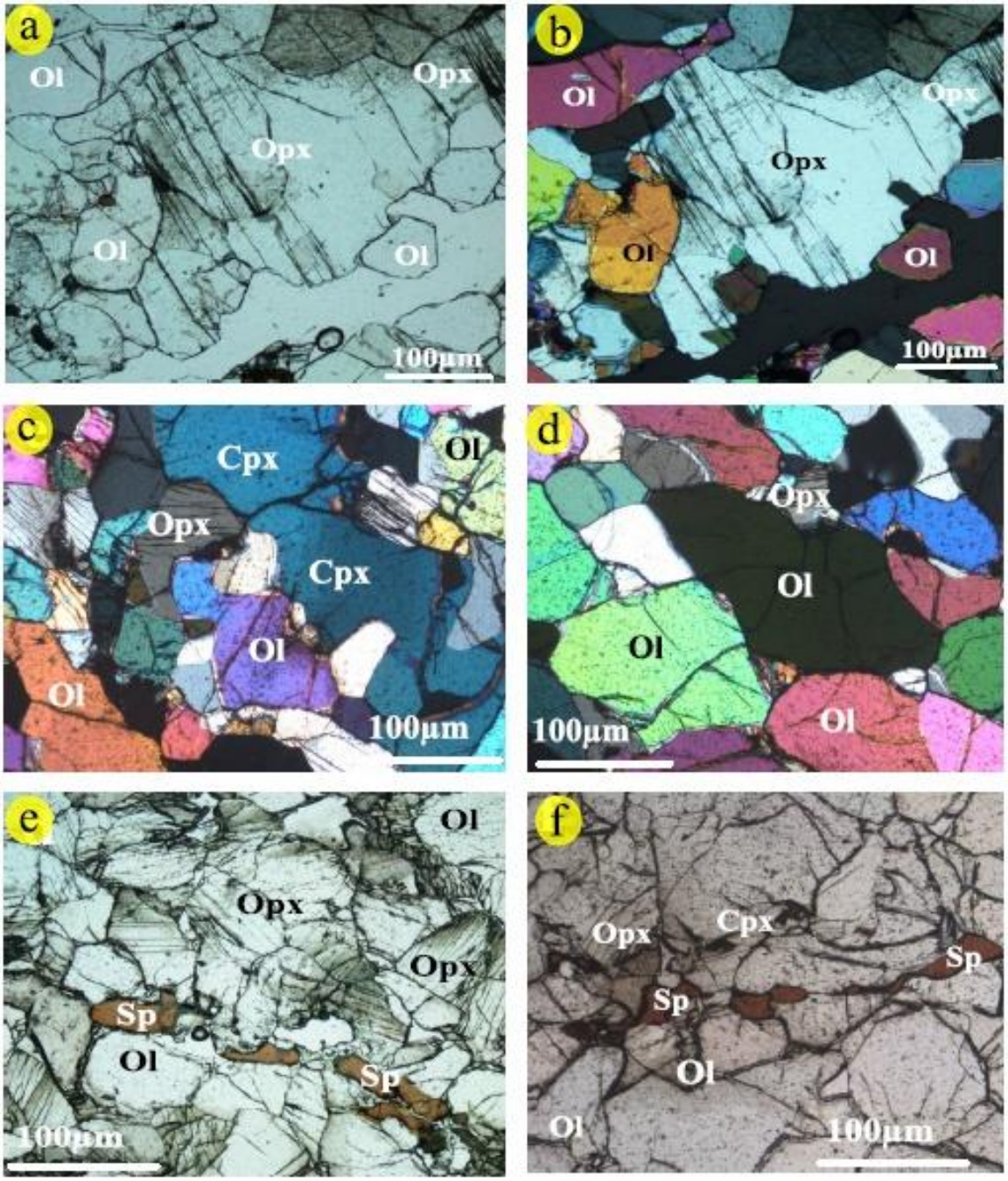

Fig. 4: Photomicrograph of mantle peridotites showing: **a** coarse- to medium-grained orthopyroxene (Opx) in Spinel harzburgite xenolith, Plain polarized light (PPL). **b** Same view of (a) crossed nicoles (CN). **c** coarse-to medium-grained clinopyroxene (Cpx) olivine, and orthopyroxene (Opx), in lherzolite xenolith, (CN). **d** coarse-grained olivine (Ol) and undulose extinction in spinel harzburgite xenolith, crossed nicoles (CN). **e** elongated spinel (Sp) grain surrounded by orthopyroxene (Opx) and olivine in spinel harzburgite xenolith, (PPL). **f** small elongated brown spinel (Sp) grain surrounded by olivine in lherzolite xenolith, (PPL).

Table 1: Representative microprobe analyses of olivine of Shawran Crater, Bir Ali peridotite xenoliths, Mg# = Mg/ ($Mg^{+}Fe^{+2}$) atomic ratio.

Rock type	Spinel harzburgites				Lherzolite			
Oxides wt%	1	2	5	24	1	2	5	6
SiO_2	41.80	41.78	41.75	41.04	40.70	40.73	39.93	40.50
TiO_2	0.02	0.01	0.00	0.03	0.03	0.01	0.01	0.01
Al_2O_3	0.01	0.03	0.03	0.02	0.01	0.02	0.01	0.01
Cr_2O_3	0.00	0.03	0.01	0.06	0.02	0.03	0.01	0.04
FeO	9.02	8.74	9.03	8.89	9.70	9.80	10.98	9.90
MnO	0.06	0.05	0.18	0.11	0.12	0.11	0.20	0.13
MgO	50.36	49.93	50.19	49.40	49.41	49.30	48.05	49.10
CaO	0.07	0.07	0.05	0.08	0.09	0.10	0.13	0.10
Na_2O	0.00	0.02	0.01	0.00	0.01	0.03	0.01	0.01
K_2O	0.01	0.00	0.02	0.00	0.01	0.01	0.01	0.01
NiO	0.30	0.35	0.45	0.32	0.31	0.35	0.41	0.30
Total	**101.63**	**101.00**	**101.72**	**99.95**	**100.39**	**100.51**	**99.75**	**100.11**
Oxyg. Atoms	**4**	**4**	**4**	**4**	**4**	**4**	**4**	**4**
Si	1.00	1.01	1.00	1.00	1.00	1.00	0.99	0.99
Ti	0.00	0.00	0.00	0.00	0.00	0.00	0.00	0.00
Al	0.00	0.00	0.00	0.00	0.00	0.00	0.00	0.00
Cr	0.00	0.00	0.00	0.00	0.00	0.00	0.00	0.00
Fe	0.18	0.18	0.18	0.18	0.20	0.20	0.23	0.20
Mn	0.00	0.00	0.00	0.00	0.00	0.00	0.00	0.00
Mg	1.80	1.80	1.80	1.80	1.80	1.80	1.78	1.80
Ca	0.00	0.00	0.00	0.00	0.00	0.00	0.00	0.00
Na	0.00	0.00	0.00	0.00	0.00	0.00	0.00	0.00
K	0.00	0.00	0.00	0.00	0.00	0.00	0.00	0.00
Ni	0.00	0.01	0.01	0.01	0.01	0.01	0.01	0.00
Total	**3.00**	**2.99**	**3.00**	**3.00**	**3.00**	**3.00**	**3.01**	**3.01**
Mg#	**0.91**	**0.91**	**0.91**	**0.91**	**0.90**	**0.90**	**0.89**	**0.90**

Table 2: Representative microprobe analyses of orthopyroxene of Shawran Crater, Bir Ali peridotite xenoliths, Mg# = Mg/ ($Mg^{+}Fe^{+2}$) atomic ratio. En= $MgSiO_3$, Wo=$CaSiO_3$, Fs= $FeSiO_3$

Rock type	Spinel harzburgites				Llherzolites			
Oxides wt%	15	18	19	22	15	18	19	22
SiO_2	56.01	56.34	56.67	56.37	55.52	55.17	55.19	55.22
TiO_2	0.05	0.04	0.05	0.07	0.09	0.10	0.14	0.08
Al_2O_3	3.31	3.29	3.27	3.22	3.76	4.06	3.50	3.70
Cr_2O_3	0.41	0.51	0.42	0.41	0.39	0.30	0.40	0.37
FeO	5.55	5.35	5.21	5.61	5.90	6.04	7.02	5.80
MnO	0.14	0.09	0.10	0.10	0.14	0.15	0.12	0.11
MgO	33.38	33.42	33.62	33.87	33.65	33.43	33.60	34.05
CaO	0.77	0.75	0.68	0.77	0.70	0.70	0.80	0.75
Na_2O	0.06	0.07	0.05	0.05	0.04	0.05	0.00	0.04
K_2O	0.02	0.01	0.01	0.00	0.00	0.01	0.01	0.00
NiO	0.06	0.13	0.01	0.08	0.10	0.06	0.06	
Total	**99.75**	**99.99**	**100.08**	**100.55**	**100.25**	**100.11**	**100.84**	**100.18**
Oxyg. Atoms	**6**	**6**	**6**	**6**	**6**	**6**	**6**	**6**
Si	1.93	1.94	1.94	1.93	1.91	1.90	1.90	1.90
Ti	0.00	0.00	0.00	0.00	0.00	0.00	0.00	0.00
Al	0.13	0.13	0.13	0.13	0.15	0.17	0.14	0.15
Cr	0.01	0.01	0.01	0.01	0.01	0.01	0.01	0.01
Fe	0.16	0.15	0.15	0.16	0.17	0.17	0.20	0.17
Mn	0.00	0.00	0.00	0.00	0.00	0.00	0.00	0.00
Mg	1.72	1.71	1.72	1.73	1.73	1.72	1.72	1.75
Ca	0.03	0.03	0.02	0.03	0.03	0.03	0.03	0.03
Na	0.00	0.00	0.00	0.00	0.00	0.00	0.00	0.00
K	0.00	0.00	0.00	0.00	0.00	0.00	0.00	0.00
Ni	0.00	0.00	0.00	0.00	0.00	0.00	0.00	0.00
Total	**4.00**	**3.99**	**3.99**	**4.00**	**4.01**	**4.01**	**4.02**	**4.02**
Mg#	**0.91**	**0.92**	**0.92**	**0.91**	**0.91**	**0.91**	**0.90**	**0.91**
En	**89.47**	**88.97**	**88.80**	**89.92**	**90.69**	**90.78**	**90.79**	**92.24**
Fs	**9.06**	**9.60**	**9.91**	**8.62**	**7.95**	**7.86**	**7.65**	**6.30**
Wo	**1.48**	**1.43**	**1.28**	**1.46**	**1.36**	**1.37**	**1.55**	**1.46**

Table 3: Representative microprobe analyses of clinopyroxene of Shawran Crater, Bir Ali peridotite xenoliths, Mg# = Mg/ ($Mg^{+}Fe^{+2}$) atomic ratio. En= $MgSiO_3$, Wo=$CaSiO_3$, Fs= $FeSiO_3$

Rock type	Spinel harzburgites				Llherzolites		
Oxides wt%	4	11	12	20	4	11	12
SiO_2	53.31	50.94	53.32	52.88	51.98	52.03	51.44
TiO_2	0.21	0.96	0.19	0.33	0.32	0.39	0.77
Al_2O_3	4.69	6.10	4.51	4.76	5.28	5.52	4.89
Cr_2O_3	1.00	2.04	1.03	0.92	0.77	0.63	0.58
FeO	2.07	1.82	2.06	2.28	2.37	2.53	2.58
MnO	0.08	0.02	0.06	0.02	0.08	0.07	0.16
MgO	16.21	16.31	16.21	16.22	16.22	16.22	16.83
CaO	21.48	21.31	21.46	21.23	21.46	21.40	20.70
Na_2O	1.06	0.74	1.10	1.24	1.08	1.02	0.85
K_2O	0.02	0.00	0.01	0.00	0.00	0.01	0.01
NiO	0.03	0.09	0.05	0.00	0.04	0.06	0.05
Total	**100.14**	**100.33**	**99.99**	**99.88**	**99.60**	**99.88**	**98.86**
Oxyg. Atoms	**6**	**6**	**6**	**6**	**6**	**6**	**6**
Si	1.92	1.84	1.93	1.91	1.89	1.89	1.88
Ti	0.01	0.03	0.01	0.01	0.01	0.01	0.02
Al	0.20	0.26	0.19	0.20	0.23	0.24	0.21
Cr	0.03	0.06	0.03	0.03	0.02	0.02	0.02
Fe	0.06	0.05	0.06	0.07	0.07	0.08	0.08
Mn	0.00	0.00	0.00	0.00	0.00	0.00	0.00
Mg	0.87	0.88	0.87	0.87	0.88	0.88	0.92
Ca	0.83	0.83	0.83	0.82	0.84	0.83	0.81
Na	0.07	0.05	0.08	0.09	0.08	0.07	0.06
K	0.00	0.00	0.00	0.00	0.00	0.00	0.00
NiO	0.00	0.00	0.00	0.00	0.00	0.00	0.00
Total	**4.00**	**4.00**	**4.00**	**4.01**	**4.01**	**4.01**	**4.01**
Mg#	**0.93**	**0.94**	**0.93**	**0.93**	**0.92**	**0.92**	**0.92**
En	**49.1**	**49.8**	**49.2**	**50.1**	**50.4**	**50.1**	**51.7**
Fs	**4.2**	**3.4**	**4.0**	**2.8**	**1.7**	**2.4**	**2.7**
Wo	**46.7**	**46.8**	**46.8**	**47.1**	**47.9**	**47.5**	**45.7**

Table 4: Representative microprobe analyses of spinel of Shawran Crater, Bir Ali peridotite xenoliths, Cr# (= Cr/(Cr + Al) atomic ratio.

Rock type	Spinel harzburgites						Llherzolite			
Oxides wt%	3	37	50	39	21	22	3	7	9	10
SiO_2	0.03	0.03	0.02	0.01	0.02	0.01	0.12	0.47	0.10	0.10
TiO_2	0.04	0.03	0.04	0.02	0.04	0.07	0.07	0.16	0.15	0.14
Al_2O_3	48.36	49.22	46.90	47.82	45.62	42.10	54.99	56.98	55.10	53.10
Cr_2O_3	20.14	19.43	20.84	22.47	23.95	28.03	13.44	11.38	14.80	11.50
FeO	10.07	9.83	9.89	9.91	9.86	8.70	9.54	9.39	10.30	13.00
MnO	0.10	0.17	0.13	0.15	0.13	0.11	0.11	0.12	0.16	0.11
MgO	20.20	20.15	20.01	19.84	19.88	19.50	21.13	21.46	19.20	18.80
CaO	0.00	0.00	0.00	0.00	0.02	0.02	0.01	0.10	0.01	0.00
Na_2O	0.01	0.01	0.01	0.03	0.01	0.01	0.00	0.05	0.00	0.00
K_2O	0.03	0.00	0.01	0.00	0.00	0.00	0.00	0.01	0.00	0.00
NiO	0.19	0.33	0.25	0.20	0.17	0.20	0.38	0.38	0.31	0.35
Total	**99.19**	**99.20**	**98.08**	**100.44**	**99.69**	**98.74**	**99.81**	**100.50**	**100.13**	**99.10**
Oxyg. Atoms	**4**	**4**	**4**	**4**	**4**	**4**	**4**	**4**	**4**	**4**
Si	0.00	0.00	0.00	0.00	0.00	0.00	0.00	0.01	0.00	0.00
Ti	0.00	0.00	0.00	0.00	0.00	0.00	0.00	0.00	0.00	0.00
Al	1.54	1.56	1.51	1.51	1.46	1.38	1.69	1.72	1.70	1.70
Cr	0.43	0.41	0.45	0.48	0.51	0.61	0.28	0.23	0.31	0.25
Fe2+	0.19	0.19	0.19	0.21	0.20	0.19	0.18	0.17	0.24	0.24
Fe3+	0.04	0.03	0.04	0.02	0.03	0.01	0.03	0.03	-0.02	0.05
Mn	0.00	0.00	0.00	0.00	0.00	0.00	0.00	0.00	0.00	0.00
Mg	0.81	0.81	0.82	0.79	0.80	0.81	0.82	0.82	0.75	0.76
Ca	0.00	0.00	0.00	0.00	0.00	0.00	0.00	0.00	0.00	0.00
Na	0.00	0.00	0.00	0.00	0.00	0.00	0.00	0.00	0.00	0.00
K	0.00	0.00	0.00	0.00	0.00	0.00	0.00	0.00	0.00	0.00
Ni	0.00	0.01	0.00	0.00	0.00	0.00	0.01	0.01	0.01	0.01
Total	**3.24**	**3.24**	**3.24**	**3.23**	**3.23**	**3.21**	**3.22**	**3.21**	**3.22**	**3.31**
Fe^{2+}	**0.19**	**0.19**	**0.19**	**0.21**	**0.20**	**0.19**	**0.18**	**0.17**	**0.25**	**0.24**
Fe^{3+}	**0.02**	**0.01**	**0.02**	**0.01**	**0.01**	**0.00**	**0.02**	**0.01**	**0.01**	**0.03**
Mg#	**0.81**	**0.81**	**0.81**	**0.79**	**0.80**	**0.81**	**0.82**	**0.83**	**0.75**	**0.76**
Cr#	**0.22**	**0.21**	**0.23**	**0.24**	**0.26**	**0.31**	**0.14**	**0.12**	**0.15**	**0.13**

Discussions

Oxidation and thermal state of mantle lithosphere

The geothermometer calibration models have been calculated using the olivine-spinel Mg-Fe^{2+} exchange

[25]. According to the olivine-spinel pairs [25], the temperature (T) of formation of peridotite xenoliths ranges between 938°C and 1,144°C, presumably at 1.5 GPa pressure. The calculation of the oxidation state (oxygen fugacity, fO_2) of the upper mantle, using the coexisting olivine-spinel associations, has been extensively applied in spinel peridotites [25]. The fO_2 values (Table 5) are given relative to the fayalite-magnetite-quartz (FMQ) buffer at 1.5 GPa [25].

The calculated fO_2 values of the studied spinel harzburgite xenoliths showed a relatively wide range, almost below the FMQ buffer ($\Delta\log fO_2$ FMQ = −2.7 to −0.97). On the fO_2 versus spinel Cr# diagram (Fig. 6), the majority of spinel harzburgite xenoliths fall within the slightly metasomatised abyssal and mid-ocean ridge basalt (MORB)-back-arc peridotite fields [4, 26]), while the lherzolite xenoliths show a narrow range of fO_2 ($\Delta\log fO_2$ FMQ = −1.7 to −0.20) and low Cr# (<0.15) and are plotted entirely within the primitive mantle composition (Fig. 6).

Thus, the spinel harzburgite xenoliths are formed under more oxidation than the lherzolite xenoliths. This indicates the heterogeneous nature of the oxidation state of the lithospheric mantle beneath the Balhaf–Bir Ali volcanic field. This also conforms with the lithospheric mantle beneath the Arabian Shield in Saudi Arabia [2, 5].

Partial melting of the Bir Ali lithospheric mantle

Peridotite xenoliths from Bir Ali can be used to characterise the lithospheric mantle beneath the rifted continental Arabian Peninsula.

Sgualdo et al. [20] and Ali and Arai [18] stated that the lithospheric mantle beneath Bir Ali is mainly composed of ordinary lherzolites and clinopyroxene-rich lherzolites, while Heikal et al. [19] stated that it is composed of spinel harzburgites.

The mineral chemistry of the spinel harzburgites is high Mg# and NiO content for olivine, high Cr_2O_3 content for clinopyroxene and orthopyroxene, and very low TiO_2 content for spinel and silicate minerals, indicating a residual origin after moderate degrees of partial melting, while high Mg# and Cr_2O_3 content for clinopyroxene and orthopyroxene as well as low TiO_2 content for spinel and silicate minerals indicate a fertile origin after low degrees of partial melting.

Cr# versus TiO_2 in spinel (Fig. 7) define a partial melting trend and distinguish between spinel that experience melt-rock interaction [27, 28, 29, 30]. The TiO_2 content in spinel harzburgites is generally very low (0.02–0.07 wt.%) with low spinel Cr# (0.20–0.31), while the TiO_2 content in lherzolites is generally low (0.07–0.16 wt.%) with also very low spinel Cr# (0.12–0.15). Figure 7 shows a partial melting trend, starting from fertile MORB, and TiO_2 rapidly decreases with a high degree of melting, while Cr# increases, but TiO_2 rapidly increases with a low degree of melting, and Cr# decreases.

The trend for spinel harzburgites is higher, more than 10%, while lherzolites have a generally low degree of melting, less than 8%. Spinel Cr# correlates with the Fo content of coexisting olivine. These compositional variations are interpreted to have been caused by partial melting and the mantle source. In general, the spinel Cr# and olivine Fo content increases slightly with the degree of partial melting [5]. The Cr# of spinel (0.12–0.15) and the Fo content of olivine ($Fo_{89–90}$) in the lherzolite mantle xenoliths as well as the Cr# of spinel (0.20–0.31) and the Fo content of olivine (Fo_{91}) in the spinel harzburgite mantle xenoliths are entirely plotted within the OSMA, which was interpreted as a mantle peridotite restite trend [23] (Fig. 5d).

The lherzolite and spinel harzburgite mantle xenoliths from different tectonic settings clearly occupy distinct parts of the OSMA field. The melting curve displays the percentage of melting of a fertile MORB mantle (FMM) from [29] (dashed black line, Fig. 5d) that extends through the centre of the OSMA plot [23]. This shows that lherzolites were produced by <10% melting, whereas spinel harzburgites were produced by 10–15% melting, which is consistent with the estimate based on the Cr# versus TiO_2 plot. Hellebrand et al. [31] calculated the fractional melt percentage as a function of spinel Cr#, yielding the following relationship: F = 10 × ln (Cr#) + 24, where F = melt percentage. Based on the model of [31], Bir Ali lherzolites reflect 3–5%, which was the most similar to the primitive mantle source (FMM), produced by low degrees of partial mantle melting, while the harzburgite xenoliths gave 8–12% melt extraction, which was the most similar to the melt–depletion signatures of harzburgite xenoliths, consistent with the abyssal peridotites produced by intermediate degrees of partial mantle melting [26] rather than fore-arc peridotites (Fig. 5d). Thus, the fertile lherzolite may represent an earlier deeper event with low partial melting degrees (3–5%), while harzburgite represents a later shallower event with higher partial melting degrees (8–12%) [2, 4, 5, 26, 29, 32, 33].

Comparison with mantle xenoliths from other Arabian Shield volcanic fields (Harrat Kishb)

There are clear similarities between the morphological, mineralogical, and chemical compositions of the studied mantle xenoliths and those from other parts of the Arabian Shield volcanic fields (such as Harrat Kishb), which were all formed during the Quaternary period of the Earth's history.

Morphologically, the Bir Ali and Arabian Shield volcanic fields have similar basaltic lava flows that appear as cinder cone complexes.

Petrologically, the Bir Ali volcanic field enclosing mainly mantle xenoliths of lherzolites, harzburgites, and dunites. The Arabian Shield volcanic fields (Harrat Kishb), on the other hand, host mainly of lherzolites and harzburgites with minor wehrlites [2].

Mineralogically, the Bir Ali and Arabian Shield mantle xenoliths are composed of high-Mg olivine, diopside (clinopyroxene), enstatites (orthopyroxene), and spinel.

Geochemically, Bir Ali xenoliths have high forsterite (Fo_{89}–Fo_{91}), high clinopyroxene Mg# (0.90–0.94), and variable spinel Cr# (0.12–0.31, atomic ratio), while Arabian Shield mantle xenoliths have higher forsterite (Fo_{90}–Fo_{92}), high clinopyroxene Mg# (0.91–0.93), and variable spinel Cr# (0.10–0.49, atomic ratio) [2].

The diverse population of mantle xenoliths in the Arabian Shield volcanic fields has suggested a significant lithospheric heterogeneity within the Red Sea extensional terrane [2, 5, 34].

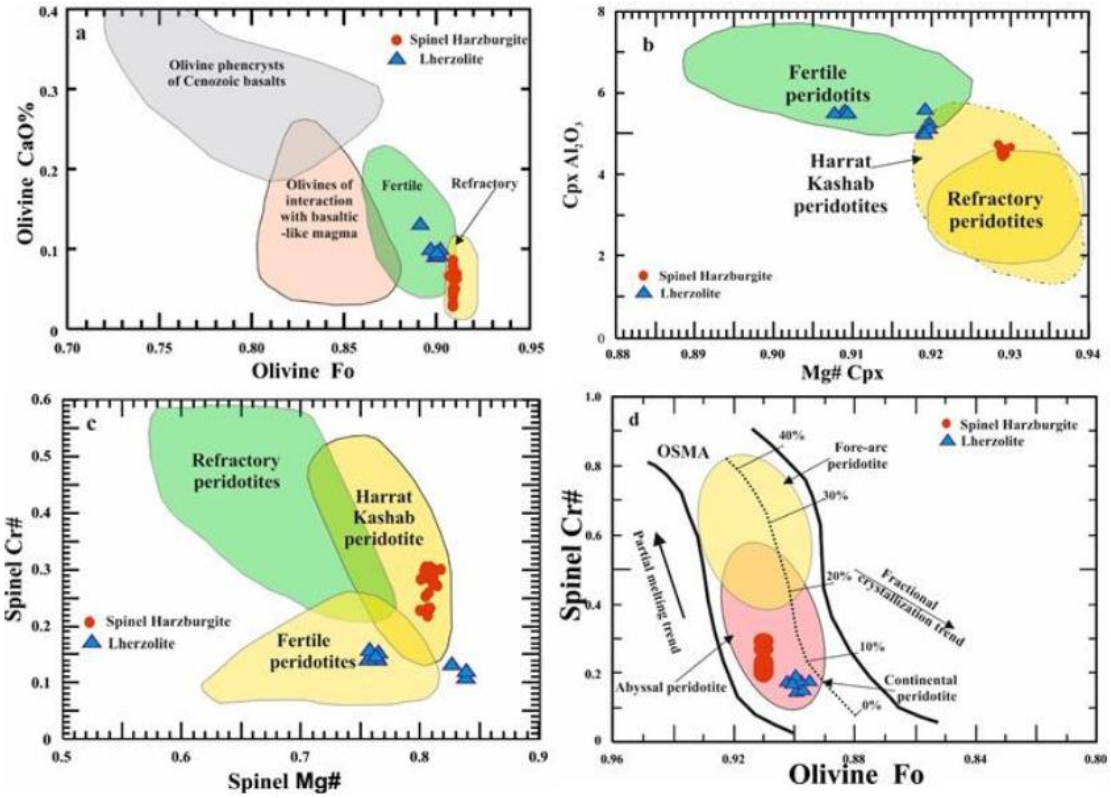

Fig. 5: Binary variation diagrams of mantle xenoliths of Bir Ali volcanism: **a** forsterite (Fo = 100×Mg#) vs CaO contents in olivine. **b** Mg# (= Mg/(Mg + Fe_t) atomic ratio) vs Al_2O_3 content of Cpx in mantle xenoliths. **c** Mg# vs Cr# (= Cr/(Cr + Al) atomic ratio) of spinel. **d** Tectonic discrimination diagram of Cr# vs Fo (atomic ratios) of the olivine-spinel pairs. The compositional fields for fertile and refractory mantle (a, b and c) are from [30, 35], and the field of Harrat Kishb mantle peridotite xenoliths is from [2]. The olivine-spinel mantle array (OSMA), melting trends and the percentage of melting in are from [23]. The abyssal, fore-arc and continental peridotites are from [26, 29, 24, 32].

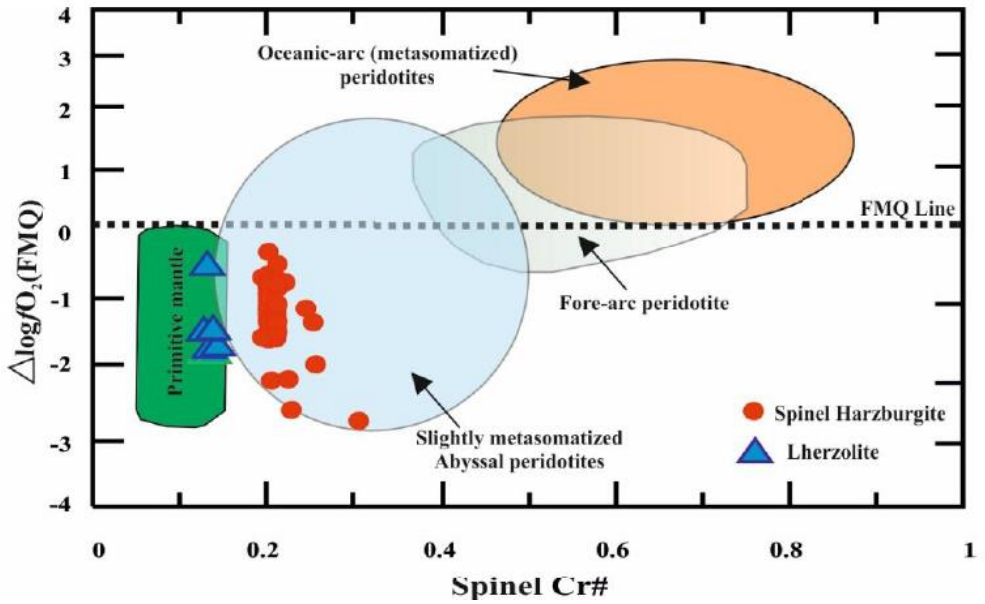

Fig. 6: Oxidation state of the studied mantle xenoliths represented by Δlog fO_2 (FMQ) vs spinel Cr#. Discrimination tectonic fields of various mantle peridotites are from [26, 32, 36].

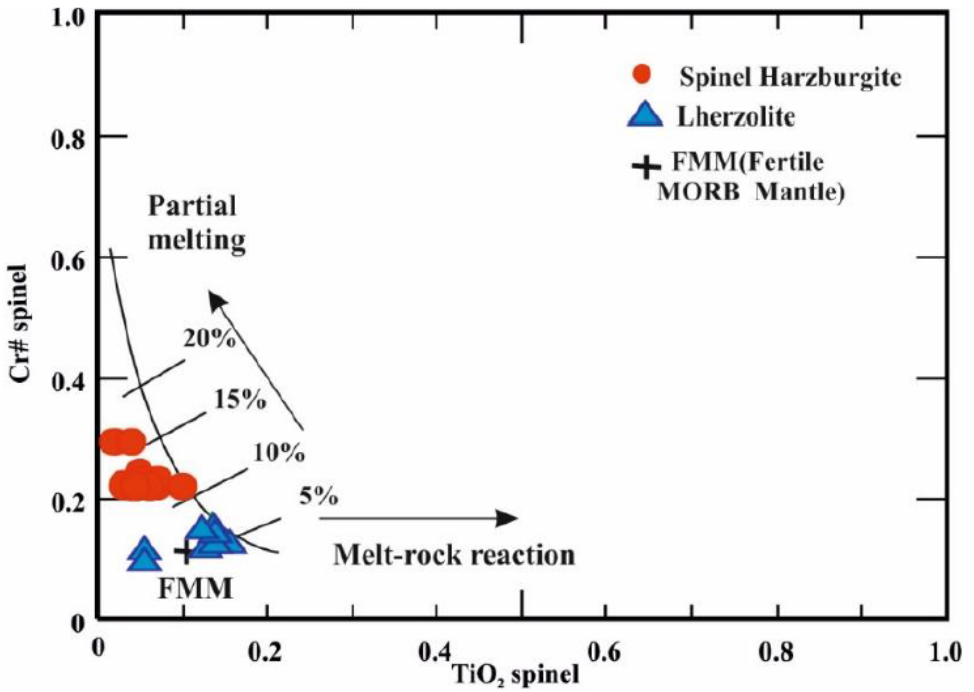

Fig.7: Binary variation diagrams of Cr# versus TiO_2 wt.% of mantle xenoliths of Bir Ali volcanism, the partial melting, melt–rock reaction trends are from [29, 30].

Table 5: Summary of minimum-maximum of temperature, oxygen fugacity and degree of melting of mantle xenoliths from Bir Ali and Harrat Kishb.

Mantle xenoliths	Sp Cr# Ballhaus et al. (1991)	Δlog fO2 Ballhaus et al. (1991)	T (°C)Ol-Sp Ballhaus et al. (1991)	F Hellebrand et al. (2001)	Reference
Lherzolites	0.12- 0.15	(-0.20)- (-1.76)	820 - 832	3 -5	This study
Harzburgites	0.20- 0.31	(-0.98) - (-2.70)	982- 1145	8 -12	
Lherzolites	< 0.20	(-0.55)- (-2.27)	813 - 938	2 - 6	[2]
Harzburgites	0.20- 0.41	(-1.34) - (-2.65)	974 – 1147	10-16	

Electronic Journal of University of Aden for Basic and Applied Sciences
EJUA-BA Vol. 3 No. 3 (2022)
https://doi.org/10.47372/ejua-ba.2022.3.185
ISSN: 2708-0684

Conclusions

- Based on petrological, geochemical, and mineralogical composition, there are two types of fresh mantle xenoliths within the Shawran Crater of the Bir Ali volcanic field: lherzolites and spinel harzburgites.
- The lherzolite xenoliths represent a fertile mantle formed by a low degree of partial melting (3–5%), while the spinel harzburgites represent a residual mantle formed by a moderate degree of partial melting (8–12%).
- Lherzolite xenoliths are characterised by Mg-rich olivine (Fo_{89}–Fo_{91}) and low Cr# (0.12–0.15). The oxidation state is almost below the FMQ buffer line ($\Delta \log fO_2$ FMQ = −0.20 to −1.76) with temperatures of about 820–832°C.
- Spinel harzburgite xenoliths are characterised by Mg-rich olivine (Fo_{90}–Fo_{91}) and moderate Cr# (0. 20-0.31). The oxidation state is almost below the FMQ buffer line ($\Delta \log fO_2$ FMQ = −0.98 to −2.70) with temperatures of about 982−1,145°C.
- The diverse mantle xenoliths in the Balhaf–Bir Ali volcanic field suggests lithospheric heterogeneity and conforms with the Arabian Shield volcanic fields.

Acknowledgment

The authors are grateful to Dr. Salah Al Khirbash and Ahmed Hassan Ahmed for reviewing and their comments that help us to improve the manuscript.

References

[1] R. J. Sewell, B. J. Hobden, S. D Weaver. Mafic and ultramafic mantle and deep crustal xenoliths from Banks Peninsula, South Island, New Zealand. New Zealand Journal of Geology and Geophysics,Vol. 36:223-231, 1993.

[2] A.H. Ahmed, A.K.M. Moghazi, M.R. Moufti, Y.H. Dawood, K.A. Ali. Nature of the lithospheric mantle beneath the Arabian Shield and genesis of Al-spinel micropods:evidence from the mantle xenoliths of Harrat Kishb, Western Saudi Arabia. Lithos 240–243, 119–139, 2016.

[3] L. Beccaluva, G. Bianchini, R.M. Ellam, C. Natali, A, Santato,. F. Siena, F.M. Stuart. Peridotite xenoliths from Ethiopia: inferences about mantle processes from plume to rift settings. Geol. Soc. Am. (GSA) Spec. Pap. 478, 77–104, 2009.

[4] U. Raye, E.Y. Anthony, R.J. Stern, J. I. Kimura, M. Ren, C. Qing, K. Tani, Composition of the mantle lithosphere beneath south-central Laurentia: evidence from peridotite xenoliths, Knippa, Texas. Geosphere, 7:710–723, 2011.

[5] A.H. Ahmed, S. Abdallah, K.A. Ali. M. Ren. Nature and evolution of the Precambrian lithosphere beneath the Arabian Shield of Saudi Arabia deduced from a suite of xenoliths from the Harrat Hutaymah Cenozoic volcanic field. Lithos 344–345 1–21. 2019.

[6] M. Wilson. Igneous petrology: a global tectonic approach. Oxford University Press, Great Britain, p 466, 1989.

[7] S.C. Bergman. Historical review in: Nixon, P. H., ed. Mantle xenoliths. A. Wiley-inter-science, NewYork, pp: 5-9. 1987.

[8] D. Carswell, and F. Gibbs. Evolution of mineral thermometer and barometer applicable to garnet Iherzolite assemblage contrib. Mineral. Petrol., 95:499-511. 1987.

[9] F.J. Spera. Carbon dioxide in petrogenesis 3: Role of volatiles in the ascent of alkaline magma with special reference to xenoliths-bearing mafic lava Contrib. Mineral. Petrol., 88:217-232. 1984.

[10] T. Rooney, T. Furman, G. Yigu and D. Ayalew. Structure of the Ethiopian lithosphere: Xenoliths evidence in the main Ethiopian Rift. Geochemical et Cosmochica Acta, 69:3889-3910. 2005.

[11] H. Al-Fugha and M. AL-Amaireh. Petrology and Origin of Ultramfic Xenoliths from North Eastern Jordan Volcanoes. American Journal of Applied Sciences, 4 (7): 491-495. 2007

[12] A.T. Al-Mishwat, and T.T. Dawod. Geochemistry and Petrogenesis of Basaltic Rocks and Enclosed Xenoliths from the Ghab Pliocene Volcanic Field in Northwestern Syria. International Journal of Geosciences, 12:667-688, 2021. https://www.scirp.org/journal/ijg.

[13] M. A. Mattash, L. Pinarelli, O.Vaselli, A. Minissale, M. C. Jaimes-Viera, M. Al-Kadasi, M. N. Shawki and F.Tassi,. Geochemical Evolution of Southern Red Sea and Yemen Flood Volcanism: Evidence for Mantle Heterogeneity," Arabian Journal of Geosciences, 7(11):4831-4850. 2014. DOI:10.1007/s12517-013-1120-1.

[14] M.A. Mattash, L. Pinarelli, O. Vaselli, A. Minissale, M. Al-Kadasi, M.N. Shawki, F.Tassi. Continental flood basalts and rifting: Geochemistry of Cenozoic Yemen Volcanic Province. International Journal of Geoscience, 4(10):1459-1466. 2013.

[15] M. A. Mattash, and K. Balogh. K-Ar Radiometric Age Data on Cenozoic Volcanics and Their Associated Terti- ary Intrusions from Yemen. Acta Mineralogica-Petro- graphica, 35:83-92. 1994.

[16] H. Schramm, A. Barth, N. Barth, W. Haubold, J. Jungwirth, W. Kainz, E. Koch, O. Krentz, C. Legler, G. Legler, H. Oehme, B. Porath, R. Reissmann, H. Schlede, R. Schirn, D. Schuppel, G. Villwock, G.Weigelt, H. Wiefel, S. Zemke. Geological survey and mineral prospecting in the Habban-Mukalla area. Final report VEB(K) Gologischeforschung und Erkundung Hall (Germany) and Department of Geology and mineral Exploration Aden. Unpublished report, vol. 1. 1986.

[17] J. Baker, L. Snee, M Manzies. A brief Oligocene period of flood volcanism in Yemen: implications for the duration and rate of continental flood volcanism at the Afro-Arabian triple junction. Earth Planet Sci Lett 136:39–55. 1996a.

[18] M.Ali, S. Arai. Clinopyroxene-rich lherzolite xenoliths from Bir Ali, Yemen-possible product of peridotite/melt reactions. J. Mineral. Petrol. Sci. 102, 137–142. 2007.

[19] M.T. S. Heikal, E.M. Lebda, Y. Orihashi, A. Habtoor. Petrogenetic evolution of basaltic lavas from Balhaf-Bir Ali Plio-Quaternary volcanic field, Arabian Sea, Republic of Yemen. Arab J. Geosci 7: 69-86. 2012.

[20] P. Sgualdo, K. Aviado, L. Beccaluva, G. Bianchini, J. Blichert-Toft, J.G Bryce, F. Siena. Lithospheric mantle evolution in the Afro-Arabian domain: Insights from Bir Ali mantle xenoliths (Yemen). Tectonophysics, 650:3–17. 2015.

[21] M.J. Grolier, W. C. Overstreet. Geologic map of Yemen Arab Republic (Sana'a) US Geological SurveyMisc. Inv. Series, Map 1-1134-B, scale 1: 500,000. 1978.

[22] J.A. Baker, G. Chazot, M. Menzies, M. Thirlwall. Metasomatism of the shallow mantle beneath Yemen by the Afar plume—implications for mantle plumes, flood volcanism, and intraplate volcanism. Geology 26, 431–434. 1998.

[23] S. Arai. Characterization of spinel peridotites by olivine-spinel compositional relationships: review and interpretation. Chem. Geol. 113, 191–204. 1994.

[24] H. Dick, T. Bullen. Chromian spinel as a petrogenetic indicator in abyssal and alpine- type peridotites and spatially associated lavas. Contrib. Mineral. Petrol. 86, 54–76. 1984.

[25] C. Ballhaus, R.G. Berry, D.H. Green. High pressure experimental calibration of the olivine-orthopyroxene-spinel oxygen geobarometer: implications for the oxygen state of the upper mantle. Contrib. Mineral. Petrol. 107, 27–40. 1991.

[26] S. Arai, S. Ishimaru. Insights into petrological characteristics of the lithosphere of mantle wedge beneath arcs through peridotite xenoliths: a review. Journal of Petrology 49, 665–695. 2008.

[27] S. Arai. Chemistry of chromian spinel in volcanic rocks as a potential guide to magma chemistry: London, Mineralogical Magazine, v. 56, p. 173–184. 1992.

[28] M.F. Zhou, P.T. Robinson, J. Malpas, Z. Li. Podiform chromitites in the Luobusa ophiolite (Southern Tibet): implications for melt–rock interaction and chromite segregation in the Upper Mantle. Journal of Petrology, 37(1):3–21, 1996. DOI: 10.1093/petrology/37.1.3

[29] J.A. Pearce, P.F. Barker, S.J. Edwards, I.J. Parkinson, P.T. Leat. Geochemistry and tectonic significance of peridotites from the South Sandwich arc-basin system, South Atlantic. Contrib. Mineral. Petrol. 139:36–53. 2000.

[30] Y.G. Xu, M.A. Menzies, M.F. Thirlwall, X.L. Huang, Y. Liu, X.M. Chen. Reactive harzburgites from Huinan, NE China: products of the lithosphere–asthenosphere interaction during lithospheric thinning? Geochim. Cosmochim. Acta, 67:487–505. 2003.

[31] E. Hellebrand, J.E. Snow, H.J.B. Dick, A.W. Hoffmann. Coupled major and trace elements as indicators of the extent of melting in mid-ocean-ridge peridotites. Nature 410, 677–681. 2001.

[32] I.J. Parkinson, J.A. Pearce. Peridotites from the Izu–Bonin–Mariana forearc (ODP Leg 125): evidence for mantle melting and melt–mantle interaction in a suprasubduction zone setting. Journal of Petrology 39:1577–1618. 1998.

[33] I.J. Parkinson, and R.J. Arculus. The redox-state of subduction zones: Insights from arc-peridotites: Chemical Geology, 160: 409–423, doi: 10.1016/ S0009-2541(99)00110-2. 1999.

[34] M. Menzies. Mantle ultramafic xenoliths in alkaline magmas: Evidence for mantle heterogeneity modified by magmatic activity. In: Hawkesworth, C.J., Norry, M.J. (Eds.), Continental Basalts and

Mantle Xenoliths: Cheshire. Shiva Publishing Limited, United Kingdom, pp. 92–110. 1983.

[35] J.P. Zheng, S.Y. O'Reilly, W.L. Griffin, F.X. Lu, M. Zhang, N.J. Pearson. Relict refractory mantle beneath the eastern North China block: significance for lithosphere evolution. Lithos, 57:43–66. 2001.

[36] C. Ballhaus. Redox states of lithospheric and asthenospheric upper mantle. Contrib.Mineral. Petrol. 114, 331–348. 1993.

مقالة بحثية

دراسة الزينولث من الوشاح في البازلت البليوسيني الرباعي من فوهة شوران، بير علي، اليمن

عبدالمنعم حبتور[1،*]، إبراهيم الاكحلي[2] و علي لشدف الخليفي[3]

[1] قسم الهندسة الجيولوجية، كلّيّة النفط والمعادن، جامعة شبوة، شبوة، اليمن
[2] قسم الجيولوجيا، كلّيّة البترول والموارد الطبيعية، جامعة صنعاء، صنعاء ، اليمن
[3] هيئة المساحة الجيولوجية، فرع شبوة، اليمن

* الباحث الممثّل: عبدالمنعم حبتور؛ البريد الالكتروني: abdelmonemhabtoor@gmail.com

استلم في: 24 أغسطس 2022 / قبل في: 25 سبتمبر 2022 / نشر في 30 سبتمبر 2022

المُلخّص

تمثل صخور الوشاح (الزينولث) ضمن صخور التف والبازلت البركاني في بركان بحيرة شوران منطقة بئر على محافظة شبوة جنوب اليمن على طول الساحل الجنوبي الشرقي لليمن مفيدة جدًا في توضيح طبيعة الوشاح الصخري أسفل المنطقة التي تتميز بالنشاط التكتوني المتصدع والنشاط البركاني خلال العصر البليوسيني- الفترة الرباعية. تتكون هذه الصخور أساسًا من الإسبنيل هارزبورجيت والليرزوليت، بالإضافة إلى الدونيت بشكل أقل بروزًا. الإسبنيل هارزبورجيت والليرزوليت عبارة عن صخور كاملة التبلور مع ظهور إسبينيل حبيبي موزع بين معادن الاولفين والأورثوبيروكسين والكلينوبيروكسين. محتوى الفورستريت من الاولفين عالي (89-91) مما يدل على منشأ هذه الصخور بقايا الوشاح المستنفذ. يكون الاورثوبيركسين في الغالب من الانستاتيت (En89-92) بينما الكلينوبيروكسين عبارة عن الدايبوسيد في التركيب. يمكن تميز الهازبورجيت بمعامل الكروم (0.20-0.31)
بينما الليرزوليت يمكن تمييزه بمعامل الكروم. (0.12-0.15) من التركيب الكيميائي والمعدني إضافة الخصائص الصخرية ان هذه الصخور تكونت من صخور مختلطة من الوشاح الخصب والمستنفذ الذي يتواجد اسفل القشرة الأرضية اسفل منطقة بئر علي.

الكلمات المفتاحية: الزينولث، اسبنل هارزبورجيت، الاستينوسفير المستنفذ، بركانيات بئرعلي، اليمن.

How to cite this article:

A. M. Habtoor, I. A. Al-Akhaly and A. S. Lashdaf, “IMPLICATIONS OF MANTLE XENOLITHS IN THE PLIOCENE-QUATERNARY BASALTS FROM THE SHAWRAN CRATER, BIR ALI AREA, YEMEN”, *Electron. J. Univ. Aden Basic Appl. Sci.*, vol. 3, no. 3, pp. 190-203, Sept. 2022. DOI: https://doi.org/10.47372/ejua-ba.2022.3.185